


## Article

# Timber Based Integrated Techniques to Improve Energy Efficiency and Seismic Behaviour of Existing Masonry Buildings

Matteo Busselli, Davide Cassol, Alessandro Prada  and Ivan Giongo \* 

Department of Civil, Environmental and Mechanical Engineering, University of Trento, Via Mesiano 77, 38123 Trento, Italy; matteo.busselli@unitn.it (M.B.); davide.cassol-1@unitn.it (D.C.); alessandro.prada@unitn.it (A.P.)

\* Correspondence: ivan.giongo@unitn.it

**Abstract:** The retrofit solutions studied herein aim to improve the seismic and energetic behaviours of existing masonry buildings to guarantee safety and the preservation of the building heritage. The retrofit consists of timber-based products (panels and strong-backs) fixed to the masonry walls using mechanical point-to-point connections; the durability and the hygrothermal performance of the solutions are guaranteed by insulation layers and membranes. The thermophysical properties of the retrofitted walls were evaluated by means of analytical and numerical analyses, considering the heat transmission in both steady and unsteady state conditions and the thermal bridge in correspondence with the corner of the wall. The in-plane seismic behaviour of the retrofitted walls was numerically investigated through nonlinear analyses. The influence of various parameters (such as masonry and insulation properties) on the performance of the retrofit solutions was analysed via parametric simulations.

**Keywords:** unreinforced masonry; seismic rehabilitation; timber panels; timber strong-backs; hybrid techniques; energy efficiency; seismic retrofit



**Citation:** Busselli, M.; Cassol, D.; Prada, A.; Giongo, I. Timber Based Integrated Techniques to Improve Energy Efficiency and Seismic Behaviour of Existing Masonry Buildings. *Sustainability* **2021**, *13*, 10379. <https://doi.org/10.3390/su131810379>

Academic Editors: Maria Rosa Valluzzi and Angelo Masi

Received: 24 August 2021  
Accepted: 13 September 2021  
Published: 17 September 2021

**Publisher's Note:** MDPI stays neutral with regard to jurisdictional claims in published maps and institutional affiliations.



**Copyright:** © 2021 by the authors. Licensee MDPI, Basel, Switzerland. This article is an open access article distributed under the terms and conditions of the Creative Commons Attribution (CC BY) license (<https://creativecommons.org/licenses/by/4.0/>).

## 1. Introduction

Recent directives from the EU Commission, such as the Energy Performance of Buildings Directive (EPBD) and the Energy Efficiency Directive (EED) [1], aim at implementing energy efficiency in buildings and encourage renovation of the existing building stock, which for the largest part was built before the introduction of any energy standards. Energy consumption, due to both heating and cooling, can be significantly reduced by improving the performance of the building envelopes, renewable technologies and innovative design. In this regard, the use of bio-based insulating materials (e.g., timber-based products) can help reduce the carbon footprint. Strategies such as those just mentioned can contribute actively to the decarbonisation (CO<sub>2</sub> emissions reduction) of the building sector and to reach the goal of Net Zero Emissions (NZE) by 2050 [2]. The retrofit techniques analysed herein are designed to improve the seismic and energetic behaviour of existing masonry buildings, with the aim of guaranteeing the safety of the occupants while preserving the building heritage thanks to integrated and fast-execution interventions. Structural, energetic, and architectural aspects must be considered simultaneously to obtain a cost-optimal renovation [3,4]. In this respect, the use of timber elements appears as promising. The structural retrofit consists of timber-based products (panels and strong-backs) connected to the masonry walls using mechanical or adhesive point-to-point connections, while the durability and the energetic performance of the intervention are guaranteed by the installation of insulation layers and membranes.

The use of timber panels for the retrofit of existing structures (Figure 1a) has been investigated in a number of works available in the literature. A detailed description of this

retrofit solution and the outcomes of preliminary numerical analyses have been reported by Giongo et al. [5], while the properties of the timber-to-masonry wall connections have been experimentally investigated by Riccadonna et al. [6] and Rizzi et al. [7] considering, respectively, dry and adhesive connections. The effectiveness of this retrofit solution has been studied by Giongo et al. [8], who has conducted onsite testing on full-scale masonry walls retrofitted with cross laminated timber (CLT) panels. Further insight has been provided by the parametric numerical study reported in Cassol et al. [9] by means of parametric analyses. Further experimental and numerical analyses on masonry walls retrofitted with timber panels have been reported by Borri et al. [10], Pozza et al. [11], Lucchini et al. [12] and Iuorio et al. [13], while the use of timber panel for the seismic strengthening of reinforced concrete structures has been investigated by Sustersic and Dujic [14,15] and by Smiroldo et al. [16,17].

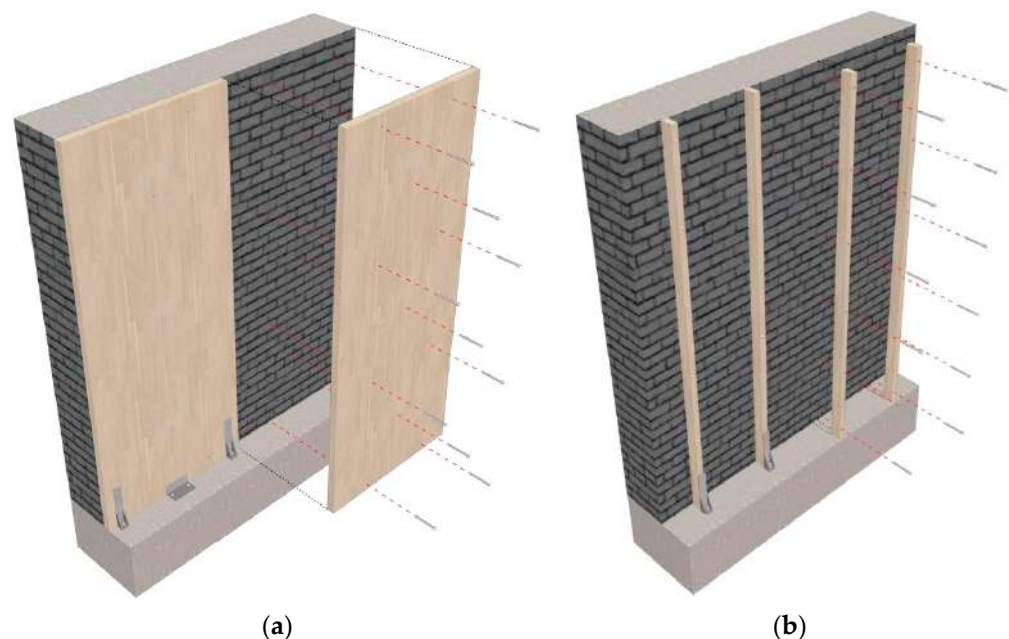


**Figure 1.** Example of timber-based retrofits for URM walls: (a) timber panel retrofit; (b) timber strong-back retrofit.

The timber strong-backs retrofit solution (Figure 1b) consists of fixing vertical timber elements, named strong-backs, to the masonry walls by means of mechanical connections, with the aim of improving the out-of-plane capacity of the unreinforced masonry (URM) walls. The effectiveness of such techniques was experimentally investigated by Giaretton et al. [18], Dizhur et al. [19], and Cassol et al. [20]. Another example of timber-based retrofit is the “timber framing and sheathing” technique, which is a hybrid solution combining strong-backs with timber sheets. Such a technique produces an increase in both the in-plane and the out-of-plane capacity of the URM walls; the technique’s effectiveness was recently tested by Guerrini et al. [21].

Most of the work in the literature focuses on evaluating the effectiveness of the solution in improving structural strength. The analysis of the state of the art highlighted a lack of investigation on the energetic aspects of the intervention, with very few works published on the topic (Valluzzi et al. [22]).

In this work, the seismic and energetic behaviours of various timber-based retrofit solutions were investigated. The thermophysical properties of the retrofitted walls (the steady state and the periodic thermal transmittances, the attenuation, the phase shift, and the thermal bridge in correspondence of the wall corner) were analytically and numerically evaluated, while the in-plane behaviour of the retrofitted walls was numerically investigated through nonlinear quasi-static analyses using the same modelling approach

adopted in [9]. The influence of different parameters on the effectiveness of the retrofit was studied considering various masonry and insulation properties, and different retrofit configurations.

## 2. Integrated Seismic and Energy Retrofit Solutions

Most of the retrofit solutions studied herein are designed to be installed on the interior surface of the walls with the aim of improving the seismic and the energetic behaviours while preserving the external façades. The structural retrofit is provided by timber-based products (panels and strong-backs) fixed to the masonry walls using mechanical or adhesive point-to-point connections. Vapour control layer, breathable and reflective membrane, insulation layer and finishing layer are added to guarantee the durability of the timber elements and to increase the hygro-thermal performance of the retrofitted system. Being the retrofit applied to the inner side of the building walls, a maximum thickness of the retrofit of 125 mm was assumed to limit the reduction of internal volume caused by the retrofit intervention. The designed solutions were then adapted, by modifying the type and position of the membranes and by using different finishing materials, to befit the alternative scenario that sees the retrofit applied to the external surfaces of the building walls.

The structural retrofit was ensured by timber panels (Figure 1a), timber strong-backs (Figure 1b), or a combination of both those structural elements (see Figure 2). Two types of timber panels were used: cross laminated timber (CLT) panels and laminated veneer lumber (LVL) panels. The features of the CLT panels considered in this work are the same as the panels employed in the experimental campaign reported in [6] and of the numerical studies reported in [5,9]. Such panels have a thickness of 60 mm and are composed by three layers of spruce timber of grade C24 [23]. The second type of panel (LVL) is produced by gluing veneers of spruce-wood 3 mm thick. The veneers can be oriented so that the fibres of all layers are parallel to each other. Alternatively, the panel layup can include veneers oriented transversally to the main direction, resulting in panels known as LVL-X. LVL-X panels were used in this study, with thickness values of 27 mm and 54 mm. The timber elements used as strong-backs have a cross section of 80 mm × 45 mm and are made of spruce LVL.

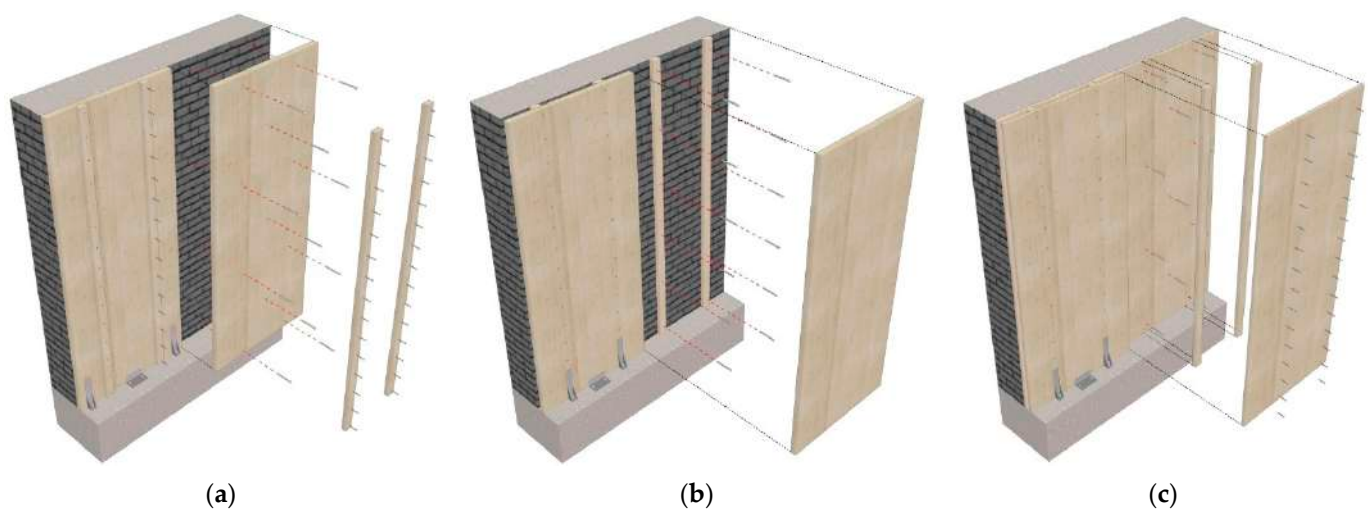


**Figure 2.** Timber-based hybrid solutions: (a) Timber panels fixed to the wall and strong-backs applied to the panel surface; (b) strong-backs fixed to the wall and timber panels fixed to the strong-backs; (c) timber panels fixed to the wall and strong-backs and additional panels fixed to the first layer of panels.

Insulation panels were employed to improve the energy efficiency of the intervention. The thickness of such panels was limited to 30 mm to minimise the reduction of internal volume due to the retrofit intervention, based on the 125 mm retrofit-thickness limit previously mentioned. Four insulation materials characterized by different values of density

and thermal conductivity were selected: wood fibre, EPS 80 (Expanded Polystyrene), EPS 100 Graphite, and aeropan (aerogel based product).

Vapour regulation is controlled by means of vapour barriers. A classification of such barriers is provided by [24] depending on the equivalent air thickness parameter ( $S_d$ ). A vapour barrier and a breathable and waterproof membrane were used to avoid condensation phenomena and rising damp problems, as well as to improve the durability of the retrofit system. Surface condensation and interstitial condensation occur when the vapour partial pressure of the moist air in a generic layer exceeds the saturation pressure at the same point. Condensation cannot be treated generically, as for transmittance, because it is highly dependent on the temperature and pressure of the external and internal environment. Every retrofit solution was analysed with the simplified Glaser's method [25] to ensure that such phenomenon did not occur, using the average monthly temperature of Trento (Italy) (alpine climate) [26], see Table 1.

**Table 1.** External and internal average monthly temperature.

	Jan.	Feb.	Mar.	Apr.	May	June	July	Aug.	Sept.	Oct.	Nov.	Dec.
$\theta_{ext}$ [°C]	0.9	2.1	7.0	11.6	16.8	19.2	22.2	21.6	17.1	11.5	5.4	0.4
$\theta_{int}$ [°C]	20.0	20.0	20.0	20.8	23.4	24.6	25.0	25.0	23.5	20.7	20.0	20.0

For all the internal solutions, a breathable and waterproof membrane was positioned on the inner side of the masonry wall to avoid imbibition phenomena due to direct contact between masonry and timber; a vapour barrier was placed on the warmer side, next to the finishing elements (e.g., plasterboard) to guarantee the thermo-hygrometric performance of the retrofit. For the external retrofit configurations, a breathable and reflective membrane was placed close to the outer finishing elements to hinder the passage of sun's rays. Furthermore, a breathable membrane was applied to the external façade of the masonry wall. Regarding the surface finishing, when the integrated retrofit intervention is done from the inside, it can be made with plasterboard or fibre-cement sheets. Differently, when the retrofit is installed on the outside surfaces, the use of fibre-cement boards and an additional layer of skim coat is preferred to guarantee the durability of the system.

A total of 35 retrofit solutions (18 internal and 17 external) were analysed. Table 2 reports the description of the adopted labelling of the retrofit solutions, Table 3 shows the horizontal cross-sections of the retrofitted walls, and Table 4 reports the thicknesses of the various layers of the retrofit.

**Table 2.** Retrofit solution labelling.

Labelling Example	Terms	Description
	CLT	CLT panel
	LVL	LVL-X panel
	SB	Strong-back
	HY	Hybrid solution
	c	Fibre-cement board
	i	Insulation
	a	Air cavity
	v	Vapour control layer (internal solution)
	t	Breathable and reflective membrane (external solution)

Note: A breathable and waterproof membrane was placed on the surface of the masonry wall in each retrofit solution. The order of the green and blue terms represents the position of the various layers starting from the surface of the masonry wall.

**Table 3.** Cross-section of the internal retrofit solutions.

CLT or LVL-X Panels	Strong-Back (80 × 45 mm)	Hybrid Solutions

Note: 1. CLT (60 mm) or LVL-X (54 mm) panel; 1\*. LVL-X (27 mm) panel; 2. Insulation layer; 3. Air cavity; 4. Skim-coating plasterboard or fibre cement panel; — breathable membrane; — vapour barrier.

**Table 4.** Layout of the internal retrofit solution: layers thicknesses and total thickness of the intervention.

ID Solution.	Elements	N° Panel	Panel THK [mm]	Insulation THK [mm]	Air Cavity THK [mm]	Plasterboard THK [mm]	+ΔTHK [mm]
CLT_1v	CLT	1	60	0	-	12	73
CLT_1iv	CLT	1	60	30	-	24	115
CLT_i1v	CLT	1	60	30	-	12	103
CLT_1iav	CLT	1	60	20	20	24	125
CLT_ia1v	CLT	1	60	20	20	12	113
LVL_1v	LVL-X	1	54	-	-	12	67
LVL_1iv	LVL-X	1	54	30	-	24	109
LVL_i1v	LVL-X	1	54	30	-	12	97
LVL_1iav	LVL-X	1	54	20	20	24	119
LVL_ia1v	LVL-X	1	54	20	20	12	107
LVL_1iv1	LVL-X	2	27	30	-	12	97
LVL_1ia1v	LVL-X	2	27	20	20	12	107
SB_80v	LVL 45 × 80	-	-	-	80	24	105
SB_80iav	LVL 45 × 80	-	-	60	20	24	105
HY_1iav	LVL-X+80 × 45	1	54	30	15	24	124
HY_ia1v	LVL-X+80 × 45	1	54	30	15	12	112
HY_1ia1v	LVL-X+80 × 45	2	27	30	15	12	112
HY_1ia1vc	LVL-X+80 × 45	1	27	30	15	30	103

### 3. Numerical Analyses

#### 3.1. Energy Performance Analyses

The improved energy performance of the 35 retrofit solutions was studied. The analyses were conducted using both analytical and numerical approaches. Additionally, the influence of the masonry wall properties and the insulation features on the energy performance were investigated through parametric simulations.

The thermophysical properties of the material used in the analyses are reported in Table 5. The masonry wall properties were selected by means of standard codes [27] and literature review considering the most common masonry types of central Italy [28].

**Table 5.** Thermophysical properties of the materials used in the analyses.

Materials	$\rho$ [kg/m <sup>3</sup> ] <sup>1</sup>	$\lambda$ [W/(mK)] <sup>2</sup>	$c_p$ [J/(kgK)] <sup>3</sup>	$\mu$ [-] <sup>4</sup>	Sd [m] <sup>5</sup>
CLT panel	420	0.120	1600	60	-
LVL panel	530	0.130	2720	60	-
Aerogel panel	230	0.015	1000	5	-
Wood fibre panel	265	0.048	2100	5	-
EPS80	15	0.037	1450	30	-
EPS100 Graphite	17	0.031	1450	50	-
Clay brick masonry	1800	0.800	840	6	-
Limestone masonry	2200	1.700	1000	200	-
Tuff masonry	1600	0.550	1000	20	-
Plasterboard	1000	0.250	2000	10	-
Fibre-cement board	950	0.300	1000	40	-
Skim-coating	950	0.310	950	13	-
Plaster	1800	0.900	910	10	-
Vapour barrier	1330	0.390	1700	$2.6 \times 10^7$	3900
Breathable membrane	250	0.300	1800	67	0.02
Breathable and reflective membrane	300	0.300	1800	100	0.05

<sup>1</sup> Density. <sup>2</sup> Conductivity. <sup>3</sup> Mass specific heat at constant pressure. <sup>4</sup> Water vapour resistance factor. <sup>5</sup> Equivalent air thickness.

The energy performance of the 35 retrofit solutions were estimated through some key performance indicators (KPI) aimed at quantifying the wall performance in winter and summer. Specifically, the thermal transmittance  $U$  [29], the periodic thermal transmittance  $Y_{ie}$  (period of 24 h), the attenuation  $fd$  and the phase shift  $\Delta T$  of the retrofitted walls were determined analytically as indicated in [30]. Moreover, the thermal bridges [31] in correspondence of the corner of the retrofitted walls were evaluated for the better performing solutions using the finite elements software THERM [32]. With such software the total heat transfer coefficient  $U_{factor}$  and the linear thermal transmittance  $\psi$  of a bi-dimensional system (see Equation (1)) are determined by solving the heat equation (Equation (2)). The domain was discretized into non-overlapping square elements and subsequently converted into quadrilaterals and triangles. The mesh size was selected so that the percentage error on the energy flux estimation was limited to a maximum of 10% in each element, while the internal and external temperatures ( $T_{int} = 20$  °C and  $T_{ext} = 0$  °C) were imposed as boundary conditions.

$$\psi = \left( U_{factor,i} \cdot l_i \right) - \sum_{j=1}^N (U_j \cdot l_j) \quad (1)$$

$$\lambda \left( \frac{d^2 T}{dx^2} + \frac{d^2 T}{dy^2} \right) + q_g = 0 \quad (2)$$

#### 3.2. Mechanical Pushover Analyses

The mechanical behaviour of the retrofitted walls was numerically investigated using the finite element (FE) software Abaqus/Explicit [33]. The modelling approaches

adopted herein were previously described and validated by the authors in [9]. The finite element model shown in Figure 3 is representative of the models used for carrying out the parametric study.

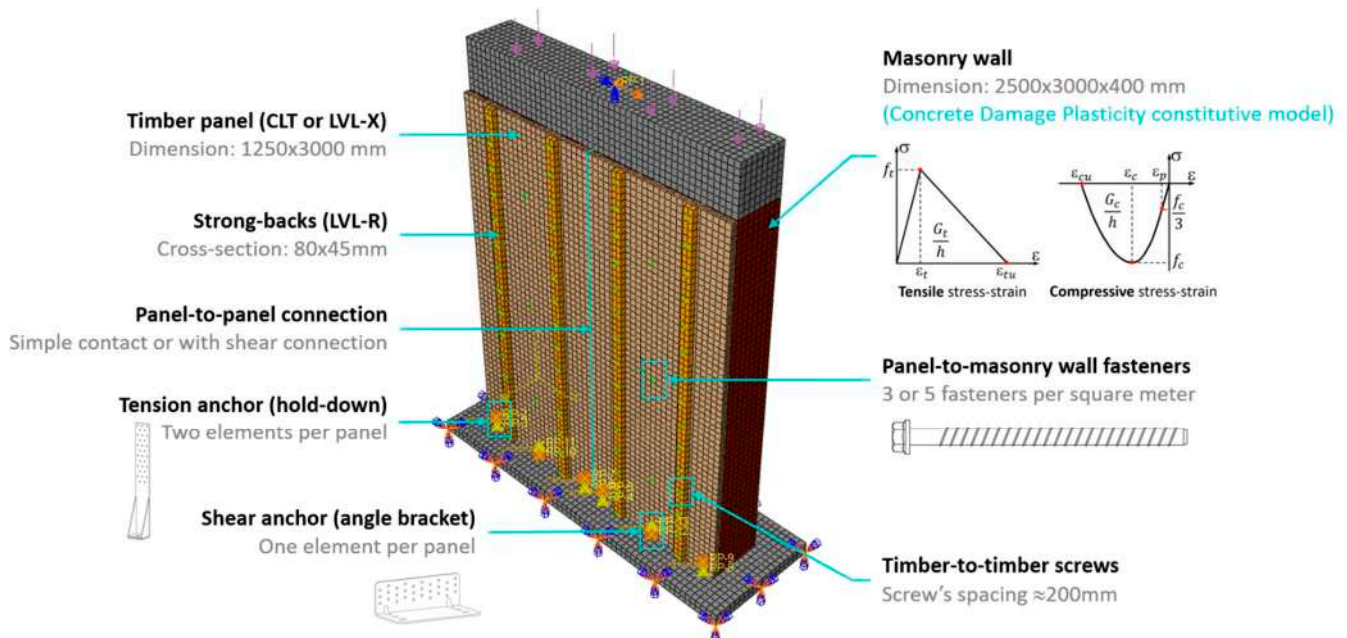


Figure 3. Numerical model of a hybrid retrofit solution.

The masonry wall was 2500 mm wide ( $l$ ), 3000 mm tall ( $h$ ) and 400 mm thick ( $t$ ) and it was simulated with an equivalent, homogeneous and isotropic material. The Concrete Damage Plasticity (CDP) [34,35] constitutive model was adopted to describe the masonry post-peak behaviour, assuming a bi-linear stress–strain relation in tension and a parabolic one in compression. The material peak conditions were determined considering the masonry tensile strength ( $f_t$ ) and compressive strength ( $f_c$ ) while the post peak behaviour was based on the fracture energy in tension ( $G_t$ ) and compression ( $G_c$ ). Table 6 reports the mechanical properties of the analysed masonry walls. The mechanical parameters  $f_t$  and  $f_c$  for different masonry types were selected from the ranges of values recommended by the Italian regulation [36,37], the elastic module  $E$  was calculated as  $E = 400f_c$ , while the fracture energy values were determined as recommended by Lourenço [38].

Table 6. Mechanical mean properties of the masonry walls used in the FE analyses.

Masonry	$f_c$ [MPa]	$f_t$ [MPa]	$E$ [MPa]	$G$ [MPa]	$G_c$ [N/mm]	$G_t$ [N/mm]
Clay brick	2.600	0.075	1040	400	6.604	0.020
Limestone	2.000	0.053	800	340	5.200	0.020
Tuff	1.400	0.042	560	300	3.724	0.020

A concrete base and a concrete beam at top of the wall (cross section 400 mm  $\times$  400 mm) were modelled using an elastic and isotropic material, to facilitate the transfer of the loads to the masonry wall. A tie constraint was used to model the surface-to-surface connection between masonry and concrete to prevent any relative displacement. Timber was discretized as an orthotropic material where inelastic phenomena, such as local crushing at the panel's toe, were simulated using a plastic constitutive model. The CLT panel was implemented as a three-layer solid, with the two external layers oriented vertically and the inner layer oriented horizontally. The LVL panel was instead modelled with an equivalent homogeneous material. The CLT panels were modelled using the properties of C24 solid

timber [23], while the equivalent homogeneous properties of the LVL panels were selected according to [39].

The timber-to-masonry connections were modelled with one-dimensional wire elements. The fastener extremities were connected to the masonry wall and to the timber elements using the *coupling* constraints available in the Abaqus software library. The radial and the axial force-displacement properties of the wire elements were calibrated on the experimental outcomes reported in Riccadonna et al. [6]. The behaviour of the timber-to-masonry connections for the 60 mm CLT panel and for the 54 mm LVL panel were derived from the experimental shear-displacement curves obtained by [6] from testing 60 mm CLT panel connections.

The property of the timber-to-masonry connections for the 27 mm LVL panel were obtained by scaling the experimental results of a 40 mm LVL panel connection. A shear capacity reduction of 19% was estimated by means of the analytical formulations proposed by Johansen [40] for steel-to-timber connections with thick plates and adopted by the Eurocode 5 [41] (fasteners yield strength  $M_{yk} = 38 \text{ Nm}$ ,  $\text{CoV} = 7\%$ ). The same modelling approach used for the timber-to-masonry connections was also adopted for representing the tension and the shear anchors, the timber panel-to-panel side connection, and the timber-to-timber connections of the hybrid solutions, where the wire element properties were derived from the experimental outcomes reported in Hossain et al. [42] and Piazza et al. [43]. The panel-to-panel side connection comprises fully threaded timber screws inserted at an angle of  $45^\circ$  to the joint line (e.g., 8 mm diameter screws spaced at 200 mm), see Figure 4. A letter “X” (connection with crossed screws) was added to the first part of the solution label to represent such type of panel-to-panel connection. For those analyses where no tensile anchor at the panel-to-panel joint was simulated, the solution was identified by the letters “XA” (crossed screws and absence of the central hold-downs). The properties of the employed connections are reported in Table 7.

Dynamic quasi-static analyses were conducted to improve the convergence and to reduce the computational cost of simulations. The loads were applied with a mean velocity of 0.2 mm/s and the quasi-static condition of the analyses was verified by ensuring that the ratio between the kinetic energy and the internal energy did not exceed 1/10. The vertical load consisted of a pressure ( $\sigma_0$ ) of 0.1 MPa, while the horizontal load was applied as an imposed displacement. Gravity load and geometric non-linearity were also considered.

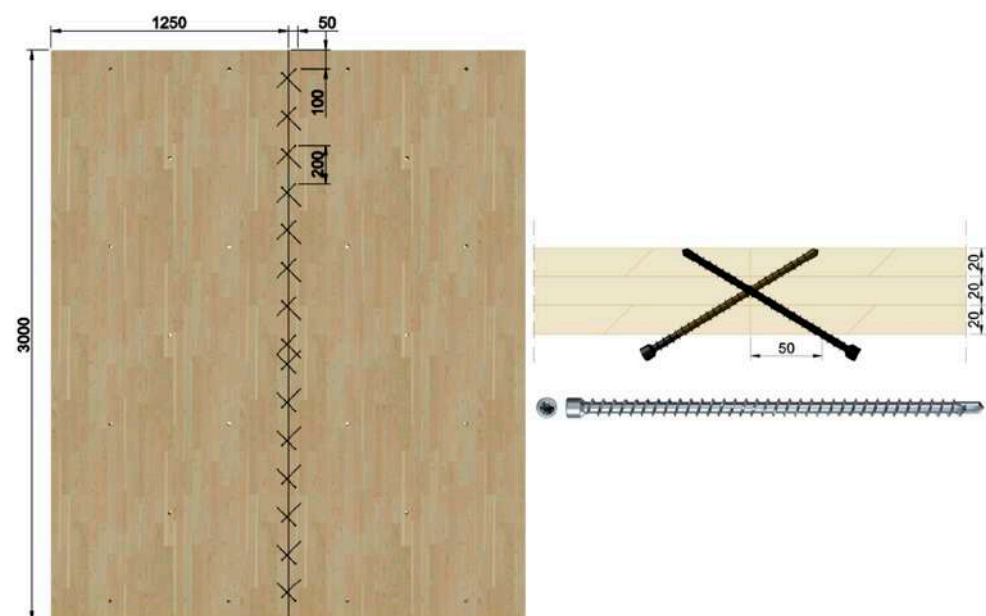


**Figure 4.** Layout of the timber screws in the panel-to-panel shear connection (dimensions in [mm]).



**Table 7.** Mechanical properties of connections.

Connection	$\varnothing$ [mm]	$d_y$ [mm] <sup>1</sup>	$K_{ser}$ [N/mm] <sup>2</sup>	$d_{max}$ [mm] <sup>3</sup>	$F_{max}$ [kN]	$d_u$ [mm] <sup>4</sup>	$F_u$ [kN]
Hold-down	-	8.92	5705	17.84	60.19	21.21	48.15
Angle bracket	-	4.23	8479	6.89	41.03	7.40	32.83
Timber-to-timber (hybrid solutions)	6	3.80	753	30.00	5.60	-	-
Panel-to-panel	8	2.00	5100	14.00	6.00	16.00	0.10

<sup>1</sup> Deformation at elastic limit. <sup>2</sup> Slip modulus. <sup>3</sup> Deformation at maximum load ( $F_{max}$ ). <sup>4</sup> Deformation at ultimate load ( $F_u$ ).

Two boundary conditions were studied, considering the wall as either fixed-free (vertical cantilever) or double fixed, to simulate the limit cases of weak and strong spandrels, and to analyse walls characterised by rocking failure (fixed-free) and shear failure (double fixed). The parametric study was conducted by varying different aspects of the retrofitted system: masonry properties, panel-to-panel side connections (with or without) and number of timber-to-masonry fasteners (3 and 5 fasteners per square meter of masonry surface). Figure 5 reports the fasteners' layouts for the analysed walls.

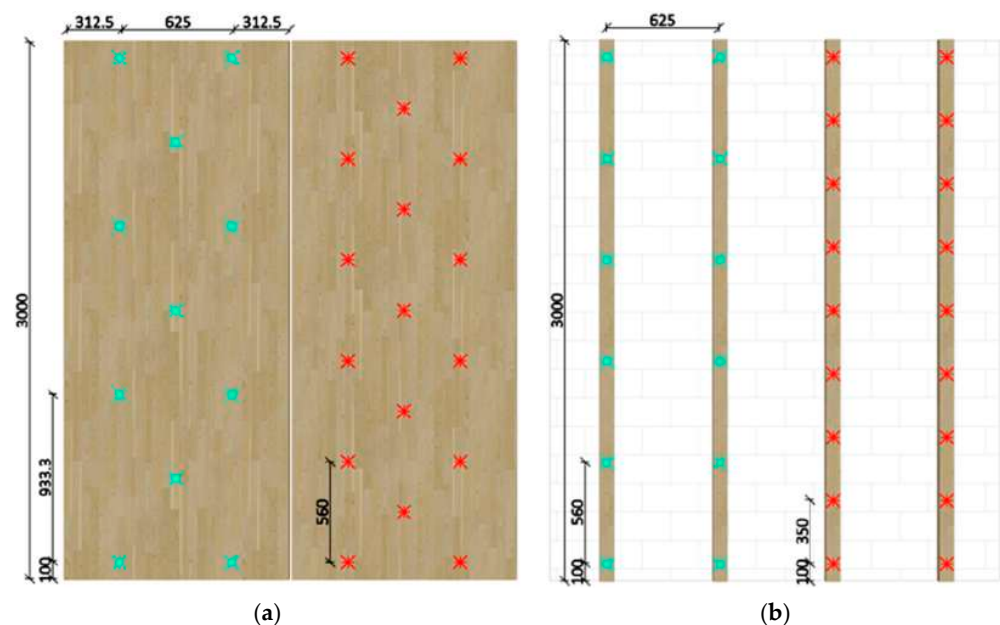


**Figure 5.** Fastener layout for the fixing patterns with 3 (in green) and 5 (in red) fasteners per square meter: (a) fastener layout for panel-to-masonry wall connection; (b) fastener layout for strong back-to-masonry wall connection.

## 4. Results

### 4.1. Energy Performance

The KPI of the retrofitted walls were analysed considering different masonry properties (Table 8), various insulation materials (Table 9) and different masonry thicknesses (Table 10). As expected, the retrofit solution *SB\_80iav* is the most effective, as it allows the installation of a greater insulation thickness while respecting the maximum thickness constraint. Additionally, the retrofit techniques with the timber panels placed close to the masonry walls, in particular the *HY\_1iav* solution, were found to be very effective. In fact, *HY\_1iav* resulted in values of the steady state ( $U$ ) and the periodic thermal transmittance ( $Y_{ie}$ ) of  $0.297 \text{ W}/(\text{m}^2\text{K})$  and  $0.008 \text{ W}/(\text{m}^2\text{K})$ , respectively. Such values were obtained assuming the best performing insulation material was used and considering the retrofit applied to a 400 mm thick clay brick masonry wall. The effect of the air layer on the thermophysical performance of the retrofitted walls was evaluated by comparing the outcomes of the solutions *LVL\_1iv* and *HY\_1iav*. It was observed that the variation of the thermophysical

properties due to the air layer has a minor effect on the effectiveness of the retrofit in the case of high-performance insulation materials (aereopan). Conversely, the variation was more noticeable when other insulation materials were employed. The effectiveness of the retrofit solution was confirmed in all the analysed configurations, characterized by different masonry walls and insulation panel properties. However, if the density of the masonry is high ( $>22 \text{ kg/m}^3$ ), the risk of superficial and interstitial condensation increases and consequently it is important to check that such phenomenon does not occur. The retrofit appeared quite promising also in the case of thin walls where high values of phase shift  $\Delta T$  ( $>12 \text{ h}$ ) were obtained.

**Table 8.** Thermophysical properties of 400 mm thick walls retrofitted with aereopan insulation panels, considering different masonry types.

	Clay Brick				Tuff				Limestone			
	U [W/(m <sup>2</sup> K)]	Yie [W/(m <sup>2</sup> K)]	fd [-]	$\Delta T$ [h]	U [W/(m <sup>2</sup> K)]	Yie [W/(m <sup>2</sup> K)]	fd [-]	$\Delta T$ [h]	U [W/(m <sup>2</sup> K)]	Yie [W/(m <sup>2</sup> K)]	fd [-]	$\Delta T$ [h]
URM400	1.41	0.196	0.139	13.22	1.07	0.086	0.081	16.09	2.25	0.332	0.147	11.69
CLT_1v	0.81	0.054	0.067	16.14	0.68	0.025	0.036	19.08	1.02	0.081	0.080	14.37
CLT_1iv	0.30	0.011	0.035	19.60	0.28	0.005	0.017	22.57	0.33	0.016	0.048	17.71
CLT_1iv	0.31	0.012	0.038	19.03	0.29	0.005	0.019	21.97	0.34	0.017	0.049	17.24
CLT_1iav	0.36	0.013	0.037	19.09	0.33	0.006	0.019	22.07	0.40	0.020	0.051	17.21
CLT_1ia1v	0.37	0.015	0.041	18.49	0.34	0.007	0.021	21.43	0.41	0.021	0.053	16.72
LVL_1v	0.86	0.052	0.060	17.07	0.72	0.024	0.033	20.02	1.12	0.082	0.073	15.26
LVL_1iv	0.31	0.008	0.026	20.69	0.29	0.004	0.013	23.66	0.34	0.013	0.038	18.82
LVL_1iv	0.32	0.009	0.027	20.37	0.30	0.004	0.014	23.31	0.35	0.012	0.035	18.58
LVL_1iav	0.37	0.011	0.029	20.21	0.34	0.005	0.014	23.18	0.41	0.017	0.041	18.33
LVL_1ia1v	0.38	0.011	0.030	19.88	0.35	0.005	0.015	22.82	0.42	0.016	0.038	18.11
LVL_1iv1	0.32	0.011	0.033	19.62	0.30	0.005	0.016	22.62	0.35	0.016	0.047	17.67
LVL_1ia1v	0.38	0.014	0.036	19.13	0.35	0.006	0.018	22.12	0.41	0.017	0.042	18.19
SB_80v	1.05	0.094	0.089	14.85	0.85	0.043	0.051	17.74	1.46	0.145	0.099	13.21
SB_80iav	0.18	0.006	0.036	19.85	0.17	0.003	0.018	22.80	0.19	0.009	0.049	18.03
HY_1iav	0.30	0.008	0.026	20.80	0.28	0.003	0.012	23.78	0.32	0.012	0.038	18.93
HY_1ia1v	0.30	0.008	0.027	20.48	0.28	0.004	0.013	23.42	0.33	0.011	0.035	18.69
HY_1ia1v	0.30	0.010	0.033	19.73	0.28	0.005	0.016	22.73	0.33	0.015	0.047	17.77
HY_1iavc	0.32	0.013	0.041	17.78	0.30	0.006	0.020	20.78	0.35	0.020	0.058	15.83

**Table 9.** Thermophysical properties of 400 mm thick clay brick masonry walls retrofitted considering different insulation materials.

	Wood Fibre Panel				EPS 80				EPS 100 Graphite			
	U [W/(m <sup>2</sup> K)]	Yie [W/(m <sup>2</sup> K)]	fd [-]	$\Delta T$ [h]	U [W/(m <sup>2</sup> K)]	Yie [W/(m <sup>2</sup> K)]	fd [-]	$\Delta T$ [h]	U [W/(m <sup>2</sup> K)]	Yie [W/(m <sup>2</sup> K)]	fd [-]	$\Delta T$ [h]
URM400	1.41	0.196	0.139	13.22	1.41	0.196	0.139	13.22	1.41	0.196	0.139	13.22
CLT_1iv	0.52	0.021	0.041	19.23	0.48	0.021	0.043	18.30	0.44	0.018	0.042	18.41
CLT_1iv	0.54	0.024	0.045	18.45	0.49	0.023	0.048	17.70	0.45	0.021	0.046	17.82
CLT_1iav	0.54	0.023	0.043	18.86	0.50	0.022	0.044	18.20	0.48	0.021	0.043	18.29
CLT_1ia1v	0.55	0.027	0.048	18.01	0.52	0.025	0.049	17.59	0.49	0.023	0.048	17.68
LVL_1iv	0.55	0.018	0.033	20.25	0.50	0.017	0.034	19.46	0.46	0.015	0.032	19.56
LVL_1iv	0.56	0.020	0.035	19.74	0.51	0.018	0.036	19.12	0.47	0.016	0.034	19.25
LVL_1iav	0.56	0.019	0.034	19.89	0.53	0.018	0.035	19.36	0.50	0.017	0.034	19.44
LVL_1ia1v	0.58	0.022	0.038	19.36	0.54	0.020	0.038	19.00	0.51	0.018	0.036	19.10
LVL_1iv1	0.56	0.022	0.040	19.25	0.51	0.021	0.042	18.38	0.47	0.019	0.040	18.48
LVL_1ia1v	0.54	0.023	0.043	18.29	0.54	0.023	0.043	18.29	0.51	0.021	0.042	18.37
SB_80iav	0.46	0.020	0.044	18.65	0.39	0.020	0.052	16.11	0.31	0.015	0.050	16.28
HY_1iav	0.50	0.015	0.030	20.56	0.46	0.015	0.032	19.56	0.43	0.013	0.031	19.65
HY_1ia1v	0.52	0.017	0.033	20.02	0.47	0.016	0.034	19.24	0.44	0.014	0.033	19.35
HY_1ia1v	0.52	0.019	0.038	19.51	0.47	0.019	0.040	18.48	0.44	0.017	0.039	18.56
HY_1iavc	0.56	0.027	0.048	17.70	0.51	0.025	0.050	16.65	0.47	0.023	0.048	16.71

**Table 10.** Thermophysical properties of 250 mm thick clay brick masonry walls retrofitted with aeropan insulation panels.

	U [W/(m <sup>2</sup> K)]	Y <sub>ie</sub> [W/(m <sup>2</sup> K)]	fd [-]	ΔT [h]
URM250	3.26	0.575	0.176	9.71
CLT_1v	0.95	0.186	0.196	11.41
CLT_1iv	0.32	0.036	0.113	14.86
CLT_i1v	0.33	0.040	0.123	14.30
CLT_1iav	0.39	0.046	0.120	14.36
CLT_ia1v	0.39	0.052	0.132	13.77
LVL_1v	1.03	0.180	0.175	12.34
LVL_1iv	0.33	0.028	0.086	15.95
LVL_i1v	0.34	0.030	0.088	15.64
LVL_1iav	0.40	0.037	0.092	15.47
LVL_ia1v	0.41	0.039	0.096	15.16
LVL_1iv1	0.34	0.037	0.109	14.88
LVL_1ia1v	0.41	0.047	0.116	14.39
SB_80v	1.31	0.326	0.249	10.11
SB_80iav	0.18	0.022	0.121	15.12
HY_1iav	0.32	0.027	0.084	16.07
HY_ia1v	0.32	0.028	0.087	15.75
HY_1ia1v	0.32	0.034	0.108	14.99
HY_1iavc	0.34	0.045	0.135	13.05

The thermal bridge in correspondence of the corner of the retrofitted walls was evaluated using the finite elements software THERM. The results were obtained by studying a 400 mm thick clay brick wall. Figures 6–12 show the trend of the infrared (IR) temperature and the heat flux, while the linear transmittance and the internal temperature of the wall corner are indicated in each figure caption and then summarized in Table 11. The heat flux results for the masonry wall corner with no retrofit are reported in Figure 6a. The comparison between Figure 6a,c shows that a single CLT panel (*CLT\_1v*) can generate an increase in the corner temperature from 13.3 °C to 15.4 °C (in the winter period), limiting the heat loss and the unevenness caused by the mortar layers.

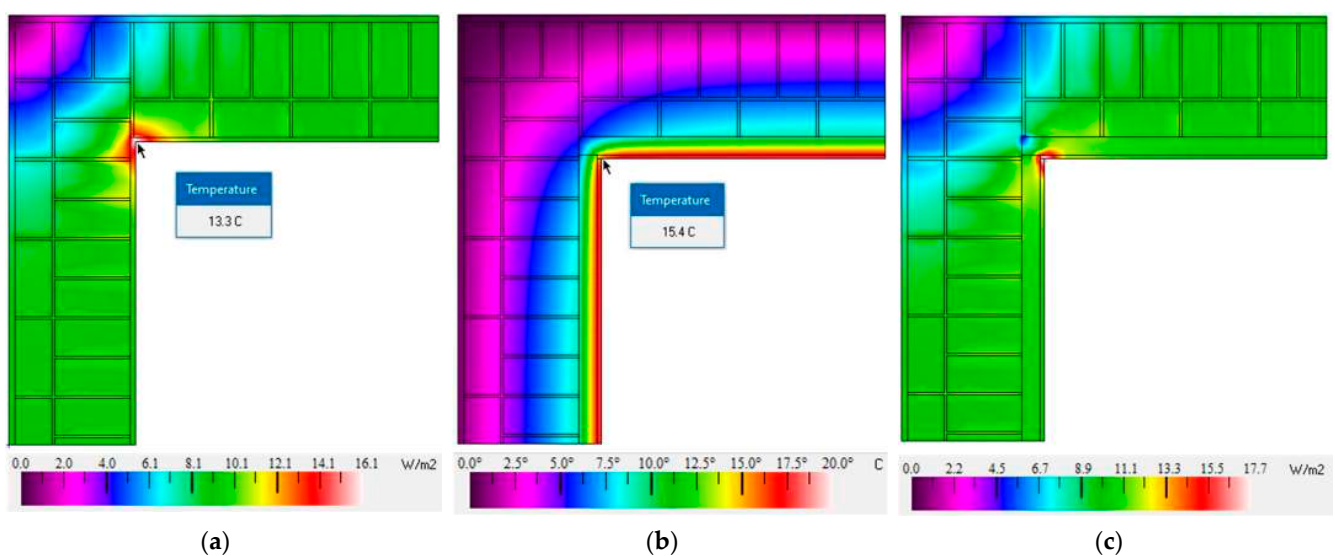


**Figure 6.** Heat flux and IR temperature trend at the wall corner: (a) URM heat flux ( $\psi = 0.412 \text{ W}/(\text{mK})$  and  $T_{\text{corner}} = 13.3 \text{ }^\circ\text{C}$ ); (b) IR temperature with *CLT\_1v* retrofit ( $T_{\text{corner}} = 15.4 \text{ }^\circ\text{C}$ ); (c) heat flux of the *CLT\_1v* solution ( $\psi = 0.229 \text{ W}/(\text{mK})$ ).

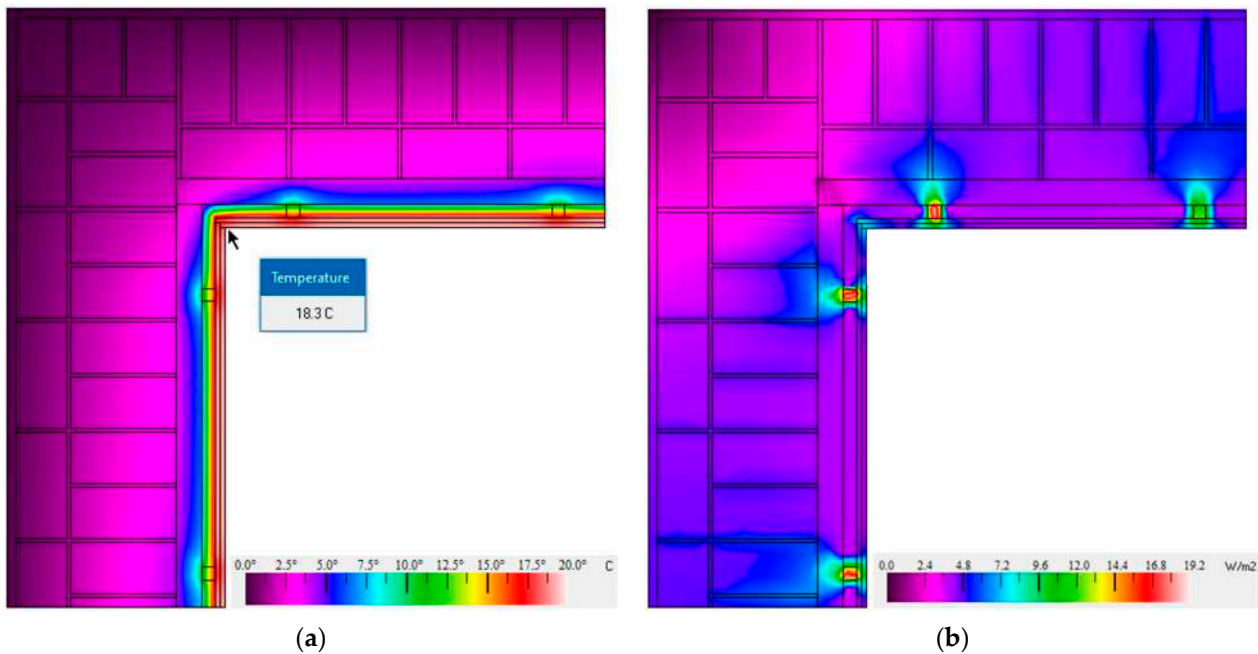


**Figure 7.** Heat flux and IR temperature trend at the wall corner: (a) IR temperature with *CLT\_1iv* retrofit ( $T_{corner} = 18.3\text{ }^{\circ}\text{C}$ ); (b) heat flux with *CLT\_1iv* retrofit ( $\psi = 0.15\text{ W}/(\text{mK})$ ). The solution *CLT\_1iv* is similar to the solution *LVL\_1iv*.

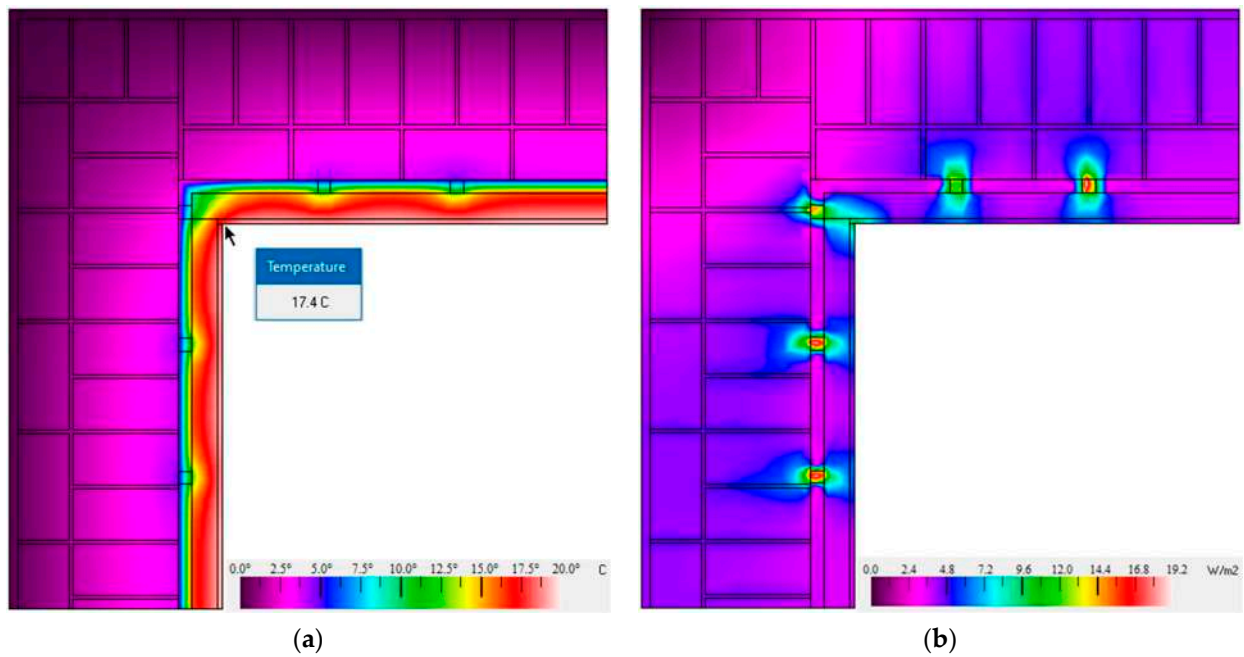


**Figure 8.** Heat flux and IR temperature trend at the wall corner: (a) IR temperature with *CLT\_i1v* retrofit ( $T_{corner} = 17.4\text{ }^{\circ}\text{C}$ ); (b) heat flux with *CLT\_i1v* retrofit ( $\psi = 0.193\text{ W}/(\text{mK})$ ). The solution *CLT\_i1v* is similar to the solution *LVL\_i1v*.

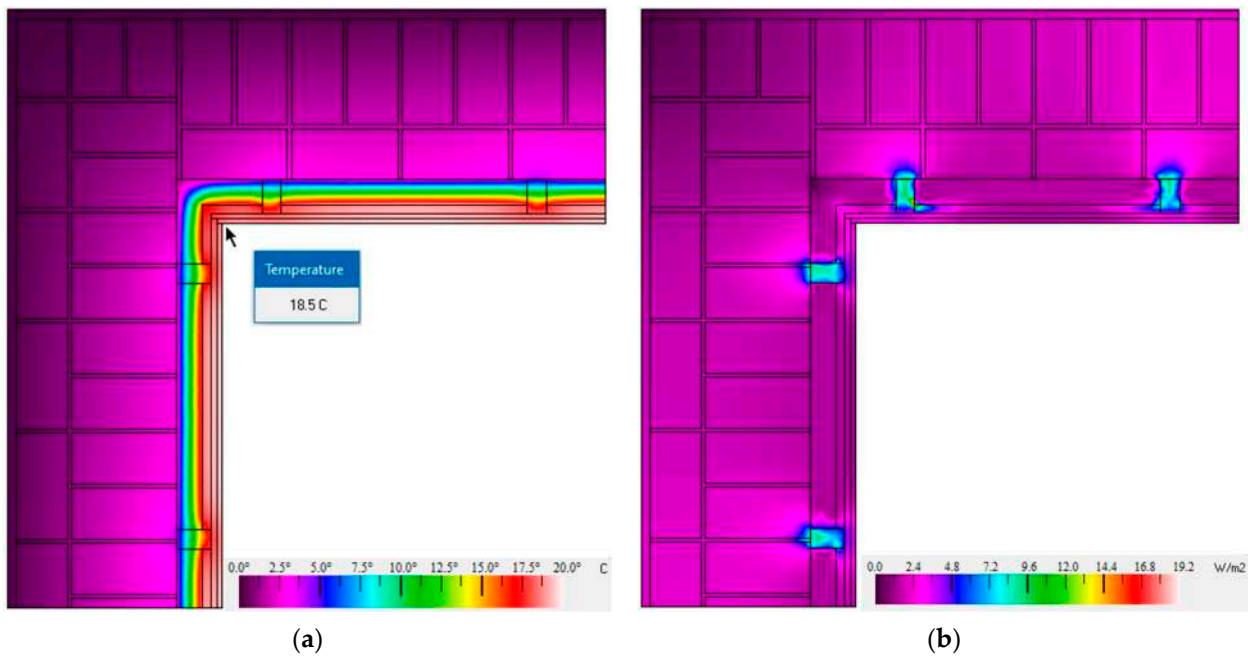


**Figure 9.** Heat flux and IR temperature trend at the wall corner: (a) IR temperature with *SB\_80iav* retrofit ( $T_{corner} = 18.5\text{ }^{\circ}\text{C}$ ); (b) heat flux with *SB\_80iav* retrofit ( $\psi = 0.256\text{ W}/(\text{mK})$ ).

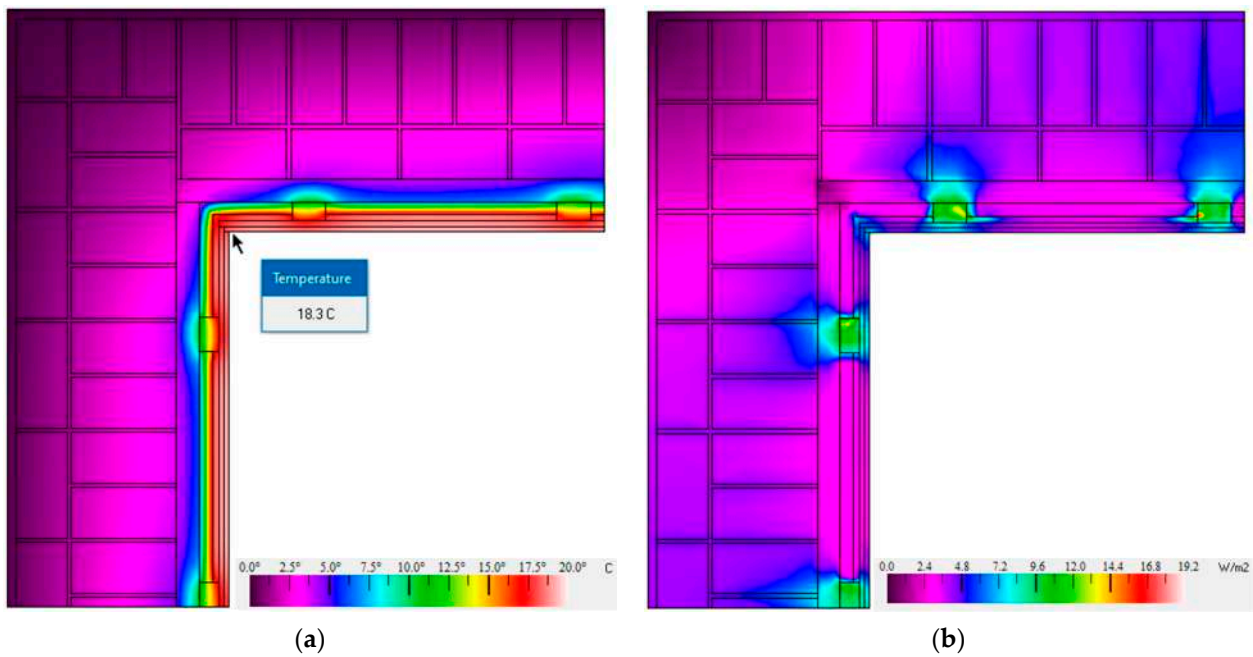


**Figure 10.** Heat flux and IR temperature trend at the wall corner: (a) IR temperature with *HY\_1iav* retrofit ( $T_{corner} = 18.2\text{ }^{\circ}\text{C}$ ); (b) heat flux with *HY\_1iav* retrofit ( $\psi = 0.232\text{ W}/(\text{mK})$ ).

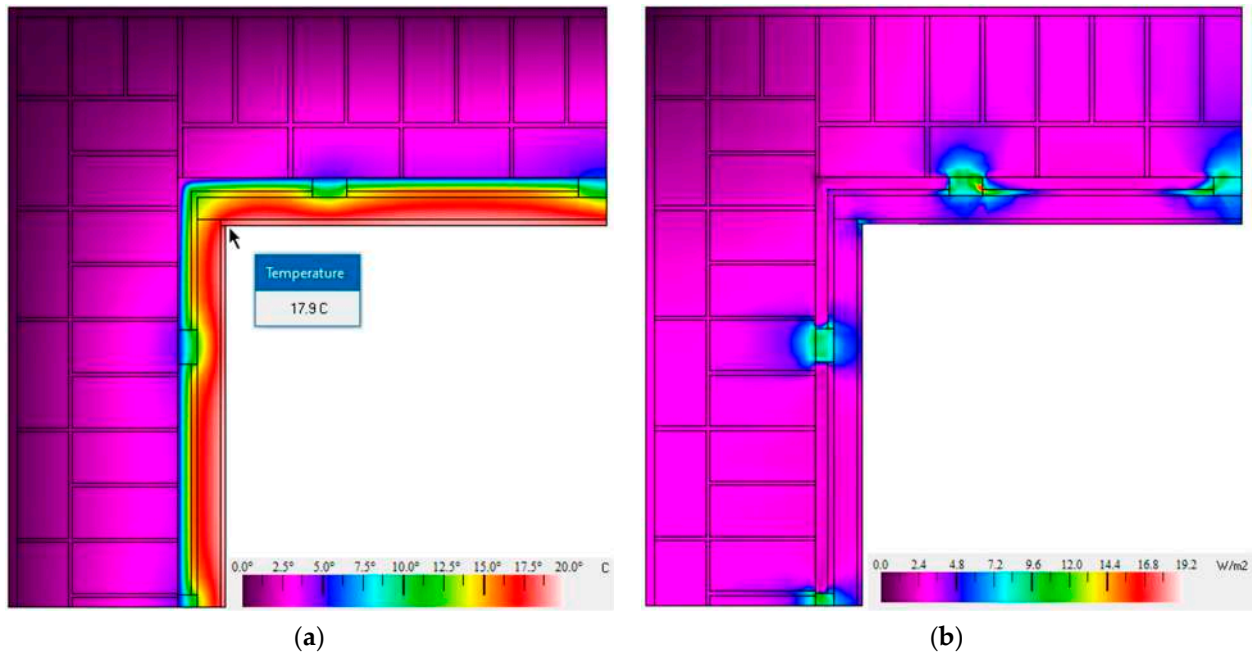


**Figure 11.** Heat flow and IR temperature trend at the wall corner: (a) IR temperature with  $HY_{ia1v}$  retrofit ( $T_{corner} = 17.9$  °C); (b) heat flux with  $HY_{ia1v}$  retrofit ( $\psi = 0.246$  W/(mK) ).

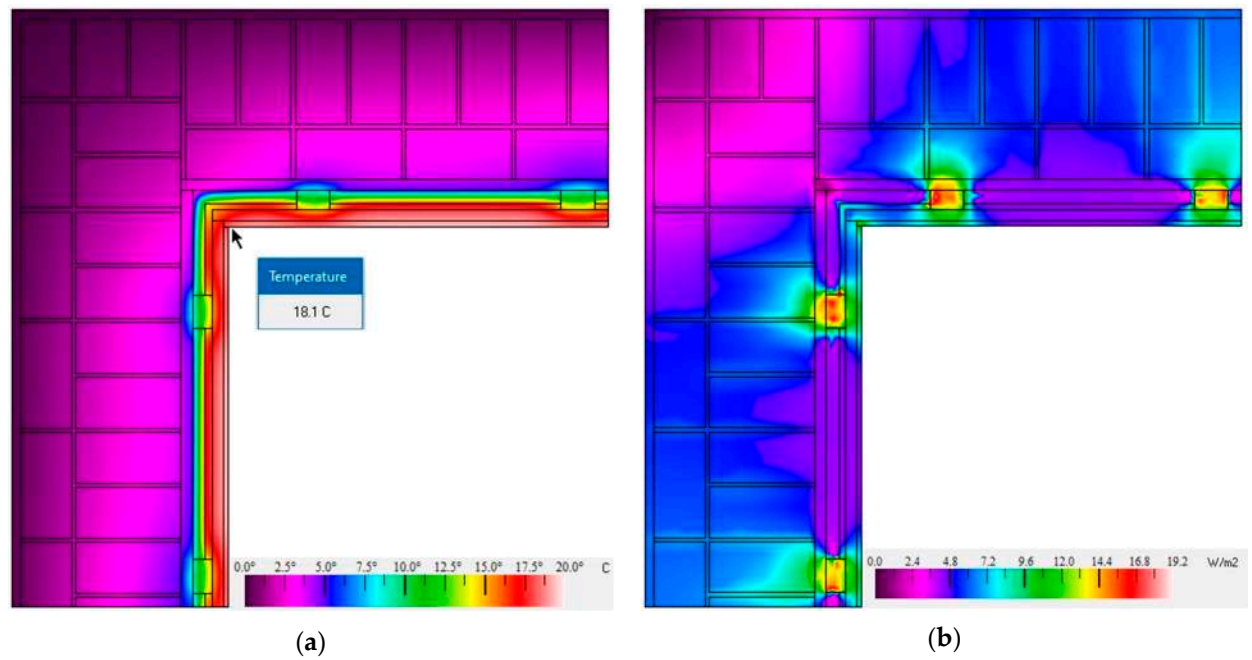


**Figure 12.** Heat flow and IR temperature trend at the wall corner: (a) IR temperature with  $HY_{1ia1v}$  retrofit ( $T_{corner} = 18.1$  °C); (b) heat flux with  $HY_{1ia1v}$  retrofit ( $\psi = 0.241$  W/(mK) ).

**Table 11.** Thermophysical properties of 400 mm thick clay brick masonry walls retrofitted with aeropan insulation panels.

	Installation Position	$T_{surf}$ [°C]	$T_{corner}$ [°C]	U [W/(m <sup>2</sup> K)]	$\psi$ [W/(mK)]	Yie [W/(m <sup>2</sup> K)]	fd [-]	$\Delta T$ [h]
URM400	-	16.5	13.3	1.41	0.412	0.196	0.139	13.22
CLT_1v	inside	17.8	15.4	0.81	0.229	0.054	0.067	16.14
CLT_1iv	inside	19.2	18.3	0.30	0.150	0.011	0.035	19.60
CLT_i1v	inside	19.2	17.4	0.31	0.176	0.012	0.038	19.03
LVL_1iv	inside	19.2	18.3	0.32	0.146	0.008	0.026	20.69
LVL_i1v	inside	19.2	17.4	0.32	0.189	0.009	0.027	20.37
SB_80iav	inside	19.5	18.5	0.18	0.256	0.006	0.036	19.85
HY_1iav	inside	19.2	18.3	0.30	0.232	0.010	0.026	20.80
HY_ia1v	inside	19.2	17.9	0.30	0.246	0.008	0.027	20.48
HY_ia1v	inside	19.2	18.1	0.30	0.241	0.010	0.033	19.73
CLT_t1	outside	17.8	15.4	0.80	0.398	0.041	0.051	16.25
CLT_ti1	outside	19.0	17.7	0.30	0.324	0.008	0.026	19.12
LVL_ti1	outside	19.0	17.7	0.31	0.324	0.006	0.020	20.22
SB_t80ai	outside	19.2	18.1	0.20	0.360	0.006	0.029	18.65
HY_tai1	outside	18.9	17.5	0.32	0.416	0.009	0.030	17.54

For all configurations with the retrofit installed on the interior surface of the walls, the presence of the insulation layer resulted in the inside surface temperature never falling below the 19 °C threshold. The minimum surface temperature was observed to be higher in solutions where the timber panels are placed close to the wall (e.g., *CLT\_1iv*, *LVL\_1iv* and *HY\_1iav*). Moreover, the temperature at the wall corner is strongly affected by the layout of the retrofit. Analytical and numerical analyses were also conducted on the configurations with the retrofit applied to the external wall surfaces and the outcomes of such simulations resulted to be consistent with the results obtained for the internal solutions. Table 11 gives the internal configuration results and includes also the best KPI for the external solutions.

#### 4.2. Mechanical Performance

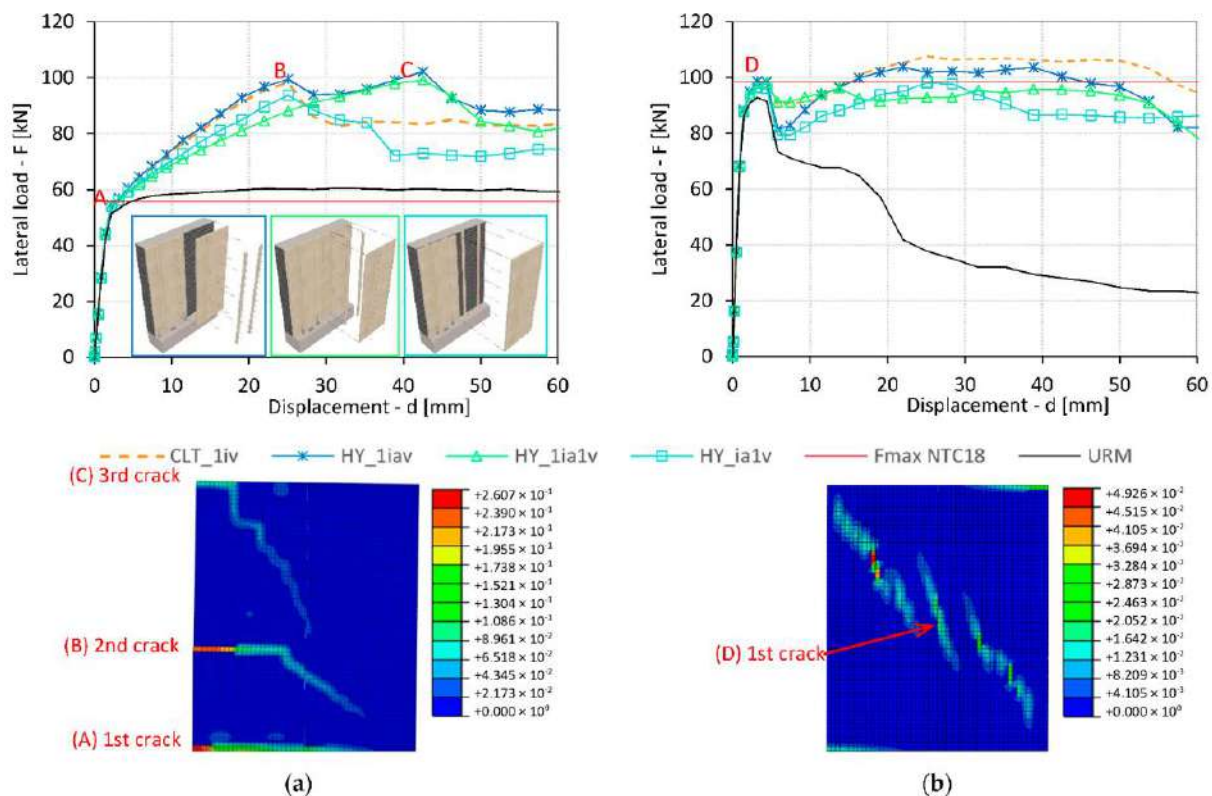
The in-plane response of masonry walls retrofitted with timber panels was previously investigated by the authors, both experimentally [8] and numerically [5,9]. Consequently, the analyses reported herein were mainly focused on the mechanical performance of the hybrid retrofit solutions. Figure 13 shows the analysis results for a masonry wall in the unreinforced and retrofitted configurations for two boundary conditions (i.e., fixed-free and double-fixed), with the retrofit characterized by no panel-to-panel side connections. The lateral load capacity of the URM wall, obtained from the FE models, is compatible with the capacity ( $F_{max}$ ) predicted using the formulations proposed by the Italian Standard [36,37] for the rocking behaviour (Equation (3)) and the diagonal shear cracking shear behaviour (Equation (4)).

$$F_{max} = \left( l^2 \cdot t \cdot \frac{\sigma_0}{2} \right) \left( 1 - \frac{\sigma_0}{0.85f_c} \right) \frac{1}{h} \quad (3)$$

$$F_{max} = \frac{(l^2 \cdot t \cdot f_t)}{h} \sqrt{1 + \frac{\sigma_0}{f_t}} \quad (4)$$

The initial branch of the lateral load–displacement curves of the retrofitted walls matched that of the unreinforced wall for both boundary conditions, confirming what reported by [5,8], that in the first phase of the loading the behaviour of the retrofitted system is governed by the masonry wall response. The contribution of the retrofit becomes noticeable after the onset of the first crack (see point A and point D). The *HY\_1iav* solution appeared to be the most effective retrofit for improving the rocking behaviour. In addition to point A, points B and C are isolated on the lateral load–displacement curve of the rocking wall retrofitted with *HY\_1iav*. Point B indicates the formation of the second crack, while point C marks the reaching of the peak lateral capacity of the retrofitted wall (102.17 kN, 43 mm) and the occurrence of the third crack. When compared to the URM configuration,

an increase in lateral load capacity of 69% was noticed at a drift value of 1.43%. It can be observed that for the shear responding wall, the application of the retrofit had an appreciable impact only on the displacement capacity (drift  $\geq 1.5\%$ ). The response curves present a small decrease in the shear capacity as soon as the wall starts cracking (point D) followed by a strength regain and a further increase. This phenomenon is due to the stiffness of the timber-to-masonry connection, requiring a 7 mm wall displacement to engage sufficient fastener shear strength to further increase the global lateral capacity. The *CLT\_1iv* and the *HY\_1iav* appeared to be the most effective solutions, with an increase in load bearing capacity larger than 10%.



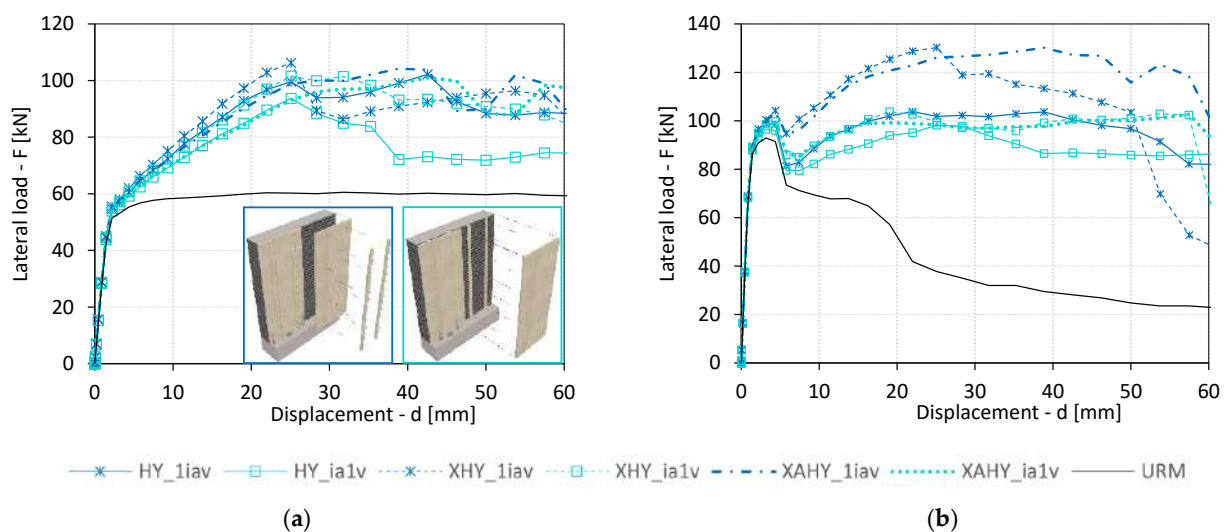
**Figure 13.** Capacity curves of retrofitted masonry walls (clay brick masonry, 3 fasteners/m<sup>2</sup>, no panel-to-panel connection) and principal strain of *HY\_1iav* solution: (a) Rocking behaviour; (b) shear behaviour.

Figure 14 presents the behaviour of masonry walls retrofitted with the hybrid solutions *HY\_1iav* and *HY\_ia1v*, accounting for the effect of the panel-to-panel side connection where fully threaded timber screws are inserted at an angle of 45° to the joint line (see Figure 4). Two sub-configurations were studied, depending on whether the base anchors (i.e., hold-downs) at the location of the panel-to-panel joint are present (letter “X” added to the labelling system) or not (letters “XA” added to the labelling system). It can be observed that for both rocking and shear cases, the lateral capacity of the X solutions is slightly smaller than that of the XA solutions. Regarding the displacement capacity, it is worth noting that in the case of wall shear failure, the X configurations showed noticeably larger values than the XA solution.

Figures 15 and 16 report the capacity curves of retrofitted walls characterized by different masonry properties and number of timber-to-masonry connections. For both failure modes, the hybrid solution with the timber panels close to the wall (*XAHY\_1iav*) resulted in the most effective. For the rocking behaviour, an increase in the number of fasteners does not produce appreciable variations in the lateral strength if the masonry has good mechanical properties (e.g., clay brick walls). On the contrary, for masonry with poor mechanical properties (e.g., tuff walls), an increase in the fastener number generates



a noticeable improvement of the effectiveness of the retrofit. The increase in lateral load capacity due to the *XAHY\_1iav* solution ranged between 30% and 60% in the case of 3 fasteners/m<sup>2</sup> and between 60% and 70% in the case of 5 fasteners/m<sup>2</sup>. Increasing the number of fasteners in the walls responding in shear provides more pronounced increases in the lateral load capacity when the masonry quality is poor, similarly to what was observed for the rocking walls. The retrofit solution *XAHY\_1iav* produced increases in the lateral load capacity between 40% and 60% in the case of 3 fasteners/m<sup>2</sup> and between 40% and 80% in the case of 5 fasteners/m<sup>2</sup>. The solution *HY\_1ia1v* was found to be the least effective, particularly in shear (appreciable increase of the displacement capacity only), due to the absence of the panel-to-panel side connection.



**Figure 14.** Capacity curves of retrofitted masonry walls (clay brick masonry, 3 fasteners/m<sup>2</sup>) for different panel-to-panel connections and anchoring configurations: (a) Rocking behaviour; (b) shear behaviour.

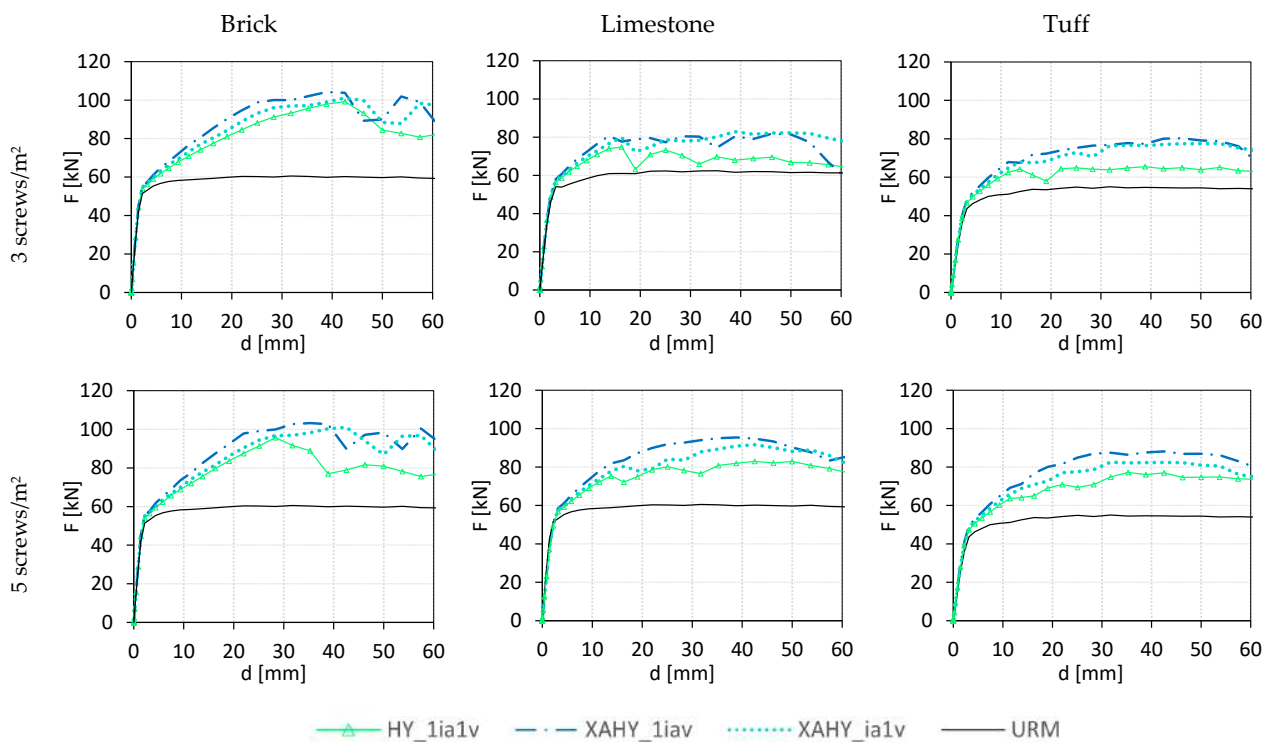


**Figure 15.** Capacity curves of retrofitted masonry walls characterized by a rocking behaviour for different masonry properties and number of fasteners.

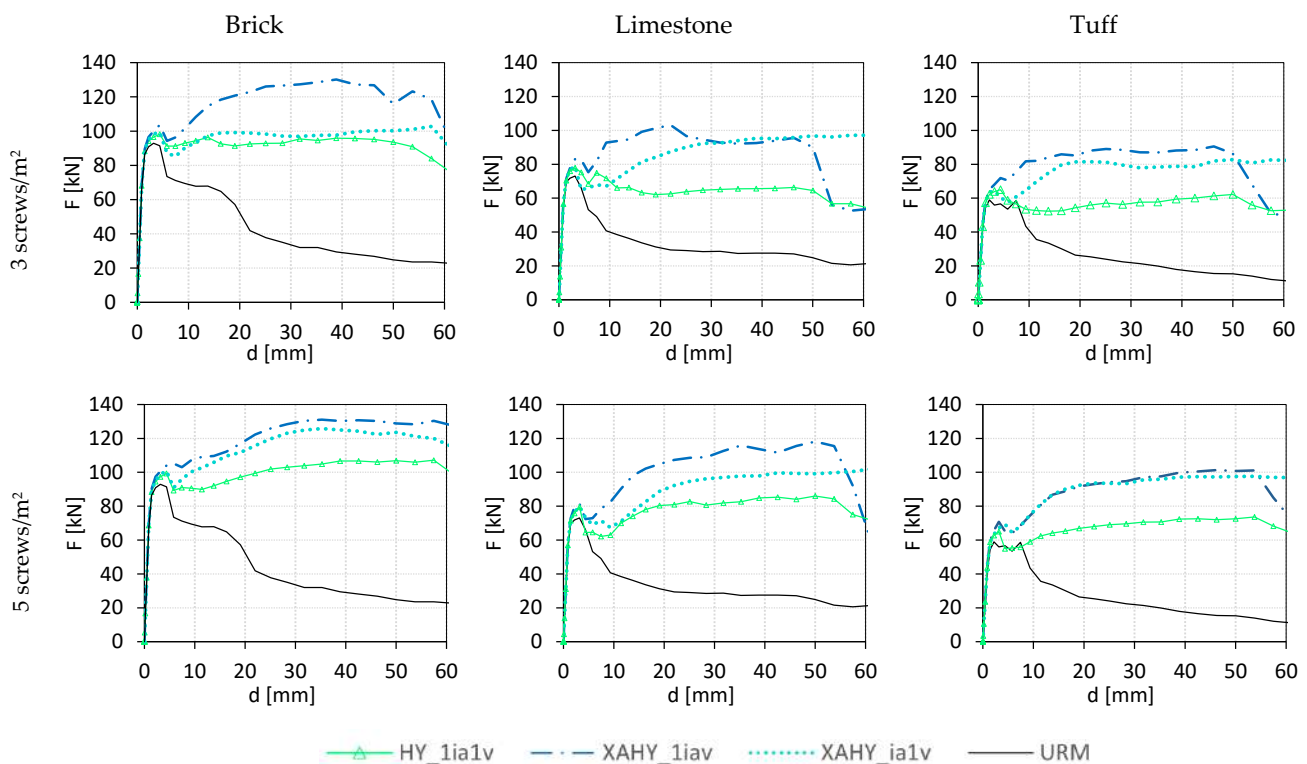


**Figure 16.** Capacity curves of retrofitted masonry walls characterized by a shear behaviour for different masonry properties and number of fasteners.

## 5. Conclusions

In this work the study of timber-based retrofit techniques for the simultaneous seismic and energy improvement of existing masonry buildings was presented. The proposed timber panel solutions reduce thermal transmittance by approximately 78% and periodic thermal transmittance by approximately 95%. Better performance was obtained with the use of strong-backs due to the larger volume of insulating material. The results showed that the retrofit configurations exhibiting the best energy performance do not change as the masonry quality and the insulating materials vary. The best performing solutions are those where the timber panels are applied closer to the wall surface. In this case, the internal surface temperature and the corner temperature are higher than in the solutions with the panels a few centimetres from the wall surface. Additionally, the analyses evidence a general increase in minimum temperature at the corners of the wall, where temperatures are close to 19 °C for many solutions. Consequently, the risk of surface condensation is reduced. As expected, the pushover analyses confirmed that the solutions with the timber panels installed on the surface of the masonry walls are also the most promising from the mechanical point of view. The retrofitted system performance can be further increased by using panel-to-panel connections. Panel-to-panel connections ensure stiffness increases for both rocking and shear behaviour, even though the best response was obtained for the walls responding in shear. As concerns the timber-to-masonry fasteners, an increase in their number generates stronger positive impacts for masonry walls with poorer mechanical properties.

To conclude, the hybrid solution with the LVL panel and the strong-backs (i.e., *HY\_1iav*) appears as the best in terms of energy performance and also from the mechanical standpoint, provided that panel-to-panel connection is used (i.e., *XAHY\_1iav*). Future developments will focus on the experimental validation of the most promising retrofit solutions studied herein. Further investigation will also be devoted to expanding the knowledge on configurations (similar to *HY\_1iavc*), that have finishing layers made of composite materials such as fibre-cement or gypsum fibre boards.

**Author Contributions:** Conceptualization, M.B., D.C., I.G., A.P.; methodology, M.B., D.C., I.G., A.P.; resources, A.P., I.G.; writing—original draft preparation, M.B., D.C.; writing—review and editing, I.G., A.P.; supervision, I.G., A.P.; funding acquisition, I.G. All authors have read and agreed to the published version of the manuscript.

**Funding:** This research received no external funding.

**Institutional Review Board Statement:** Not applicable.

**Informed Consent Statement:** Not applicable.

**Data Availability Statement:** Not applicable.

**Acknowledgments:** The research work was carried out within the framework of the 2019–2021 ReLUIS-DPC network (Italian University Network of Seismic Engineering Laboratories and Italian Civil Protection Agency). This work was supported by the Italian Ministry of Education, University and Research (MIUR) in the frame of the ‘Department of Excellence’ (grant L 232/2016).

**Conflicts of Interest:** The authors declare no conflict of interest. The funders had no role in the design of the study; in the collection, analyses, or interpretation of data; in the writing of the manuscript, or in the decision to publish the results.

## References

1. European Commission EU Buildings Factsheets. Available online: [https://ec.europa.eu/energy/eu-buildings-factsheets\\_en](https://ec.europa.eu/energy/eu-buildings-factsheets_en) (accessed on 19 July 2021).
2. International Energy Agency (IEA). Net Zero by 2050-A Roadmap for the Global Energy Sector. Available online: <https://www.iea.org/reports/net-zero-by-2050> (accessed on 19 July 2021).
3. Sbrogiò, L.; Bevilacqua, C.; De Sordi, G.; Michelotto, I.; Sbrogiò, M.; Toniolo, A.; Tosato, C. Strategies for Structural and Energy Improvement in Mid-Rise Unreinforced Masonry Apartment Buildings. A Case Study in Mestre (Northeast Italy). *Sustainability* **2021**, *13*, 8819. [[CrossRef](#)]
4. Pertile, V.; Stella, A.; De Stefani, L.; Scotta, R. Seismic and Energy Integrated Retrofitting of Existing Buildings with an Innovative ICF-Based System: Design Principles and Case Studies. *Sustainability* **2021**, *13*, 9363. [[CrossRef](#)]
5. Giongo, I.; Schiro, G.; Piazza, M. On the Use of Timber-Based Panels for the Seismic Retrofit of Masonry Structures. In Proceedings of the 3rd International Conference on Protection of Historical Constructions, Lisbon, Portugal, 12 July 2017.
6. Riccadonna, D.; Giongo, I.; Schiro, G.; Rizzi, E.; Parisi, M.A. Experimental Shear Testing of Timber-Masonry Dry Connections for the Seismic Retrofit of Unreinforced Masonry Shear Walls. *Constr. Build. Mater.* **2019**, *211*, 52–72. [[CrossRef](#)]
7. Rizzi, E.; Giongo, I.; Riccadonna, D.; Piazza, M. Testing of irregular stone masonry strengthened with cross-laminated timber. In Proceedings of the 4th International Conference on Protection of Historical Constructions, Athens, Greece, 25–27 October 2021.
8. Giongo, I.; Rizzi, E.; Riccadonna, D.; Piazza, M. On-Site Testing of Masonry Shear Walls Strengthened with Timber Panels. *Proc. Inst. Civ. Eng.-Struct. Build.* **2021**, *174*, 389–402. [[CrossRef](#)]
9. Cassol, D.; Giongo, I.; Piazza, M. Numerical Study on Seismic Retrofit of URM Walls Using Timber Panels. In Proceedings of the 8th ECCOMAS Thematic Conference on Computational Methods in Structural Dynamics and Earthquake Engineering, Athens, Greece, 27 June 2021.
10. Borri, A.; Sisti, R.; Corradi, M. Combined Reinforcement of Rubble Stone Walls with CLT Panels and Steel Cords. *Struct. Build.* **2021**, *175*, 359–371. [[CrossRef](#)]
11. Pozza, L.; Marchi, L.; Truttali, D.; Scotta, R. In-Plane Strengthening of Masonry Buildings with Timber Panels. *Proc. Inst. Civ. Eng.-Struct. Build.* **2021**, *174*, 345–358. [[CrossRef](#)]
12. Lucchini, A.; Mazzucchelli, E.; Mangialardo, S.; Persello, M. Façadism and CLT Technology: An Innovative System for Masonry Construction Refurbishment. In Proceedings of the 4th IAHS World Congress on Housing—Sustainable Housing Construction, Funchal, Portugal, 16 December 2014.
13. Iuorio, O.; Dauda, J.A. Retrofitting Masonry Walls against Out-Of-Plane Loading with Timber Based Panels. *Appl. Sci.* **2021**, *11*, 5443. [[CrossRef](#)]
14. Sustersic, I.; Dujic, B. Seismic Strengthening of Existing Buildings with Cross Laminated Timber Panels. *World* **2012**, *15*, 19.
15. Sustersic, I.; Dujic, B. Seismic Shaking Table Testing of a Reinforced Concrete Frame with Masonry Infill Strengthened with Cross Laminated Timber Panels. In Proceedings of the World Conference on Timber Engineering, WCTE 2014, Quebec, QC, Canada, 10 August 2014.
16. Smioldo, F.; Giongo, I.; Piazza, M. Seismic Retrofit of Masonry Infilled Frames by Using Timber Panel. In Proceedings of the 17th World Conference on Earthquake Engineering, Sendai, Japan, 27 September 2021.
17. Smioldo, F.; Giongo, I.; Piazza, M. Use of Timber Panels to Reduce the Seismic Vulnerability of Concrete Frame Structures. *Eng. Struct.* **2021**, *244*, 112797. [[CrossRef](#)]
18. Giaretton, M.; Ingham, J.; Dizhur, D. Timber Strong-Backs as Cost-Effective Seismic Retrofit Method for URM Buildings. In Proceedings of the NZSEE Conference, Wellington, New Zealand, 27 April 2017.

19. Dizhur, D.Y.; Giaretton, M.; Giongo, I.; Ingham, J.M. Seismic Retrofit of Masonry Walls Using Timber Strong-Backs. *SESOC J.* **2017**, *30*, 30–44.
20. Cassol, D.; Giongo, I.; Ingham, J.; Dizhur, D. Seismic Out-of-Plane Retrofit of URM Walls Using Timber Strong-Backs. *Constr. Build. Mater.* **2021**, *269*, 121237. [[CrossRef](#)]
21. Guerrini, G.; Damiani, N.; Miglietta, M.; Graziotti, F. Cyclic Response of Masonry Piers Retrofitted with Timber Frames and Boards. *Proc. Inst. Civ. Eng.-Struct. Build.* **2021**, *174*, 372–388. [[CrossRef](#)]
22. Valluzzi, M.R.; Saler, E.; Vignato, A.; Salvalaggio, M.; Croatto, G.; Dorigatti, G.; Turrini, U. Nested Buildings: An Innovative Strategy for the Integrated Seismic and Energy Retrofit of Existing Masonry Buildings with CLT Panels. *Sustainability* **2021**, *13*, 1188. [[CrossRef](#)]
23. EN 338. *Structural Timber—Strength Classes*; European Committee for Standardization: Brussels, Belgium, 2016.
24. UNI 11470:2015. *Discontinuous Roof-Synthetic, Breathable Membrane and Vapour Control Layer-Definition, Field of Application and Laying on Site*; Italian National Unification Body: Milan, Italy, 2015.
25. EN ISO 13788:2013. *Hygrothermal Performance of Building Components and Building Elements—Internal Surface Temperature to Avoid Critical Surface Humidity and Interstitial Condensation—Calculation Methods*; European Committee for Standardization: Brussels, Belgium, 2013.
26. UNI 10349:2016. *Heating and Cooling of Buildings—Climatic Data*; Italian National Unification Body: Milan, Italy, 2016.
27. UNI/TR 11552:2014. *Opaque Envelope Components of Buildings—Thermo-Physical Parameters*; Italian National Unification Body: Milan, Italy, 2014.
28. Borri, A.; De Maria, A. *WP1\_1-1\_2015UNIPG-Indice Di Qualità Muraria (IQM) e Correlazione Con Le Caratteristiche Meccaniche-Allegato 1-Linee Guida per La Compilazione Della Scheda IQM*; ReLuis: Naples, Italy, 2017.
29. EN ISO 6946:2018. *Building Components and Building Elements—Thermal Resistance and Thermal Transmittance—Calculation Methods*; European Committee for Standardization: Brussels, Belgium, 2018.
30. EN ISO 13786:2017. *Thermal Performance of Building Components—Dynamic Thermal Characteristics—Calculation Methods (ISO 13786:2017)*; European Committee for Standardization: Brussels, Belgium, 2017.
31. EN ISO 10211:2018. *Thermal Bridges in Building Construction—Heat Flows and Surface Temperatures—Detailed Calculations*; European Committee for Standardization: Brussels, Belgium, 2018.
32. *THERM and User's Manual*; Lawrence Berkeley National Laboratory (LBNL): Berkeley, CA, USA, 2017.
33. *ABAQUS Computer Software and User's Manual*; Simulia; Dassault Systèmes: Providence, RI, USA, 2017.
34. Lubliner, J.; Oliver, S.; Oñate, E. A Plastic-Damage Model for Concrete. *Int. J. Solid Struct.* **1989**, *25*, 299–326. [[CrossRef](#)]
35. Lee, J.; Fenves, G.L. Plastic-Damage Model for Cyclic Loading of Concrete Structures. *J. Eng. Mech.* **1998**, *124*, 892–900. [[CrossRef](#)]
36. Ministero delle Infrastrutture e dei Trasporti DECRETO 17 Gennaio 2018 Aggiornamento delle. In *Norme Tecniche per le Costruzioni*; Ministero delle Infrastrutture e dei Trasporti: Rome, Italy, 2018.
37. Ministero delle Infrastrutture e dei Trasporti CIRCOLARE 21 Gennaio 2019, Istruzioni per l'applicazione dell' *Aggiornamento delle "Norme Tecniche per le Costruzioni"*; Di cui al Decreto Ministeriale 17 Gennaio 2018; Ministero delle Infrastrutture e dei Trasporti: Rome, Italy, 2019.
38. Lourenço, P.B.; João, M.P. *Seismic Retrofitting Project: Recommendations for Advanced Modeling of Historic Earthen Sites*; Getty Conservation Institute: Los Angeles, CA, USA; TecMinho—University of Minho: Guimarães, Portugal, 2018.
39. EN 14279:2009. *Laminated Veneer Lumber (LVL)—Definitions, Classification and Specifications*; European Committee for Standardization: Brussels, Belgium, 2009.
40. Johansen, K.W. Theory of Timber Connections. *Int. Assoc. Bridge Struct. Eng.* **1949**, *9*, 249–262.
41. EN 1995-1-1:2014. *Eurocode 5—Design of Timber Structures—Part 1-1: General-Common Rules and Rules for Buildings*; European Committee for Standardization: Brussels, Belgium, 2014.
42. Hossain, A.; Danzig, I.; Tannert, T. Cross-Laminated Timber Shear Connections with Double-Angled Self-Tapping Screw Assemblies. *J. Struct. Eng.* **2016**, *142*, 04016099. [[CrossRef](#)]
43. Piazza, M.; Sartori, T. *Caratterizzazione Meccanica Attraverso Prove Monotone e Cicliche Dei Principali Dispositivi Di Connessione Utilizzati Negli Edifici Multipiano in Legno*; ReLuis 2015-PR4\_Allegato\_01-UR\_UNITN; ReLuis: Naples, Italy, 2015.